Article

Conformational Mechanism for the Stability of Microtubule-Kinetochore Attachments

Zsolt Bertalan,[1] Caterina A. M. La Porta,[2] Helder Maiato,[3,4] and Stefano Zapperi[1,5,*]

[1]Institute for Scientific Interchange Foundation, Torino, Italy; [2]Department of Biosciences, University of Milano, Milano, Italy; [3]Chromosome Instability and Dynamics Laboratory, Instituto de Biologia Molecular e Celular and [4]Cell Division Unit, Department of Experimental Biology, Faculty of Medicine, University of Porto, Porto, Portugal; and [5]National Research Council of Italy, Istituto per l'Energetica e le Interfasi, Milano, Italy

ABSTRACT Regulating the stability of microtubule (MT)-kinetochore attachments is fundamental to avoiding mitotic errors and ensuring proper chromosome segregation during cell division. Although biochemical factors involved in this process have been identified, their mechanics still need to be better understood. Here we introduce and simulate a mechanical model of MT-kinetochore interactions in which the stability of the attachment is ruled by the geometrical conformations of curling MT-protofilaments entangled in kinetochore fibrils. The model allows us to reproduce, with good accuracy, in vitro experimental measurements of the detachment times of yeast kinetochores from MTs under external pulling forces. Numerical simulations suggest that geometrical features of MT-protofilaments may play an important role in the switch between stable and unstable attachments.

INTRODUCTION

During mitosis, the cell equally divides into two daughter cells, with each receiving a copy of the original genetic material. Successful division requires that the two identical sister chromatids of mitotic chromosomes attach to the plus-ends of spindle microtubules (MTs) via their kinetochores (1). This process is critical, because incorrect attachments lead to mitotic errors that give rise to genetic instabilities, such as are involved in cancer (2). To ensure accurate chromosome segregation, correct MT-kinetochore attachments should remain stable while faulty attachments should be destabilized and corrected (3–5).

MTs are composed of a number of protofilaments (PFs), typically 13, and polymerize by the addition of tubulin dimers in their GTP-bound state. Growing MTs switch to a shrinkage phase when all or most GTP-bound tubulin is hydrolyzed, a process known as "catastrophe", while the switch back to a growing state is known as "rescue". These two processes constitute the dynamic instability of MTs (6). GTP-hydrolysis also induces a change in conformation of a MT protofilament from a straight to a curved state (7,8), which eventually leads to depolymerization, because curved PFs tend to peel from the MT while straight filaments remain stable. Electron micrographs of microtubules show that individual PFs can be seen curving outwards from the ends (9). Mechanical measurements of the rigidity of MTs show that their Young's modulus is two orders-of-magnitude smaller than the shear modulus (10), implying that tubulin dimers interact strongly along the PF and weakly along the transverse direction. All these structural, mechanical, and kinetic aspects have been included in theoretical and computational models that describe, with great accuracy, the main features of the stability and dynamic instability of MTs (11–15).

MT-kinetochore attachments vary in different organisms, but all seem to share a common feature (16,17): Fibrils extending from the kinetochore either link directly to curling MT-PFs, as in most higher eukaryotes (18,19), or fibrils linking to a ring, known as the Dam1 complex (20,21), form around the attached MT, as in budding yeast (22,23). Once the attachment has been formed, MT depolymerization (24) provides a force that is strong enough to carry kinetochore-attached loads (20,25,26), even in the absence of motor proteins. The precise nature of the attachment between kinetochore fibrils and MTs has been the object of intense experimental investigation. Some investigations have suggested that binding occurs through the Ndc80 complex, which interacts with tubulin by weak electrostatic forces (27). Other experiments show that the Ndc80 complex acts like a curvature sensor and binds preferentially to straight MT PFs, typical of polymerizing MTs (28). However, electron micrographs exist that vividly show kinetochore fibrils directly connecting to the tips of curling PFs (16).

In a recent article, Akiyoshi et al. (29) have shown that yeast kinetochores form "catch-bonds" with MTs. Catch-bonds become stronger under a pulling force (30,31), thus providing the possible stabilizing mechanism needed for chromosome segregation. Akiyoshi et al. also show that the kinetochore forms catch-bonds only with depolymerizing MTs, although it forms standard force-weakening bonds

Submitted October 15, 2013, and accepted for publication June 9, 2014.

*Correspondence: stefano.zapperi@cnr.it

Editor: Fazoil Ataullakhanov.

0006-3495/14/07/0289/12 $2.00

http://dx.doi.org/10.1016/j.bpj.2014.06.004

with polymerizing MTs (29). The authors gather this information into a simple two-state kinetic model that is able to fit well the experimentally measured detachment times (29). The physical mechanism by which a catch-bond forms, however, remains unclear. It is easy to understand that electrostatic interactions alone, even if protein complexes act cooperatively (27,32), would not give rise to a catch-bond: pulling charges apart leads to a weakening of the bond and should therefore increase the detachment rate. Thus electrostatic interactions reasonably account for the experimentally observed increase of detachment rate for polymerizing MTs under tension, but cannot explain at the same time the decreasing detachment rate observed for depolymerizing MTs.

Models of MT-kinetochore interactions are abundant, ranging from the classical sleeve model (33,34) to curling models (35–37), and syntheses of both (38,39), as well as incorporation of motor proteins (40), but none of them provide insight into the observed catch-bond behavior. In this article, we resolve this puzzle by combining existing experimental evidence into a model of MT-kinetochore attachment that can explain the formation of catch-bonds. We consider the interaction of a microtubule with a set of kinetochore fibrils with tips that can directly bind to straight MT-protofilaments and to neighbor fibril tips as suggested in Ciferri et al. (27) for the Ndc80 complex.

Similarly, the fibrils can be effectively cross-linked by other protein complexes such as, e.g., the Dam1 complex in budding yeast or the Mis12 complex in PtK_1 cells (18). Hence, when a polymerizing MT approaches the kinetochore, fibrils attach to its surface because of their direct interaction. This attachment is a standard force-weakening bond as expected, but the mutual interactions or cross-linking between fibrils naturally leads to the formation of fibril loops. When MTs depolymerize, the direct fibril-MT binding force is strongly suppressed (28), although the tips of curling PFs can still easily entangle in the fibril loops. This attachment is now a catch-bond, because it becomes stronger under tension. The mechanism we propose is very general and could involve other kinetochore proteins, such as CENP-E (41), CENP-T (42), and CENP-F (16), or the Ska complex (43), rather than just Ndc80, which is too short to account for the fibrils alone. The entangled organization of the fibrils observed in vertebrate kinetochores (18) provides another striking example where a velcrolike attachment, such as the one we propose, could naturally take place.

We illustrate the formation of a conformational attachment by three-dimensional simulations of a single depolymerizing MT interacting with a set of kinetochore fibrils. Once we are confident that a conformational attachment is formed, we can reduce the computational complexity of the problem by focusing on a two-dimensional representation of the interaction between a PF and a fibril loop. Numerical results of the two-dimensional model reproduce with good accuracy the catch-bond behavior reported experimentally in Akiyoshi et al. (29). We also study the stability of the MT attachment and find that it crucially depends on the local conformation of the MT. By changing the intrinsic curvature of the MT-PF, the attachment is destabilized and the catch-bond disappears. Our results suggest that the experimentally observed tension-induced stabilization of MT-kinetochore attachments could be explained by a conformational mechanism, although chemical affinities between MTs and kinetochore proteins may also play a role.

MATERIALS AND METHODS

Three-dimensional model of MT-kinetochore interactions

We construct a three-dimensional model of a MT starting from a set of wedge-shaped building blocks representing tubulin dimers, as originally suggested in Hunyadi et al. (44). A model similar in spirit to ours has been used in Cheng et al. (45) and Cheng and Stevens (46) to simulate MT self-assembly. In our model, each block is composed by eight nodes connected by stiff elastic springs, ensuring that the block behaves as a rigid object, as illustrated in Fig. 1 *a*. Diagonal springs prevent shearing and twisting of the block, while springs between nearest-neighboring nodes heavily penalize elongation and compression. The rest-length and stiffness of the springs are given in Table 1. By suitably tuning the geometrical features of the tubulin block, we can induce the desired conformation of the PFs and of the MT.

PFs are formed by arranging the blocks linearly—so that nodes 1, 2, 5, and 6 face nodes 3, 4, 7, and 8—and connecting the nodes by elastic springs with rest-length d_{10} and stiffness k_{10}, as shown in Fig. 1 *b*. When the rest-length of the springs on the top face (i.e., d_4) is equal to the rest-length of the springs on the bottom face (d_3), the PF is straight (*top*, Fig. 1 *b*), simulating the GTP-bound state. By changing d_3 so that $d_4 < d_3$, we can induce an intrinsic curvature in the PF, simulating hydrolysis into the GDP-bound state (as shown in Fig. 1 *b*).

The MT is generated by laterally aligning N PFs and connecting the blocks via springs, with rest-length d_{11} and stiffness k_{11}, to form a sheet (as shown in Fig. 1 *c*). A tubular structure is obtained by imposing the condition that the top and bottom faces of the blocks have a trapezoidal shape (as shown Fig. 1 *a*). In this condition, the PF sheet naturally folds into a cylinder, as shown in Fig. 1 *c*. We tune the geometrical parameters of the wedge so that a tubulin sheet consisting of $N \approx 11$–15 PFs will close into itself (see Table 1). A smaller number of PFs will not yield MT closure, while a larger number of PFs produces an overlapping structure. The helicity of the MT lattice is achieved by shifting the alignment of the blocks by S blocks at every turn. Although the most common case is $N = 13$ and $S = 3$ (44), here we consider $N = 13$ and $S = 2$. When the MT closes up, we clamp one end of the MT and hydrolyze or add tubulin units at the other end.

The flexural rigidity B of individual PFs in the model can be estimated from the theory of elasticity as the product of the area moment of inertia I and the elastic modulus E: $B = EI$. The area moment of inertia of a rod with a trapezoidal cross-section of height $h \approx d_5 = 2.5$ nm and top and base lengths of $d_2 = 4.55$ nm and $d_1 = 3.5$ nm is $I = d_5((d_2 + d_1)/2)^3/12 \approx 20\ \text{nm}^4$, for bending around the median line. (Values correspond to those in Mickey and Howard (47) and VanBuren et al. (14), when we consider that the total width and length of a tubulin unit is enhanced by the connecting springs, d_{10} and d_{11}, respectively.) The elastic modulus is directly related to the stiffness of the springs by $EA = 4k_{10}d_{10}$, where the factor 4 comes from the fact that we split the tension between two blocks into four parallel springs, and A is the cross-section of the block. We chose k_{10} so that B is in the range of 1.5–$50 \times 10^{-26}\ \text{Nm}^2$, which is in agreement with earlier estimates based on measurements of the bending stiffness of

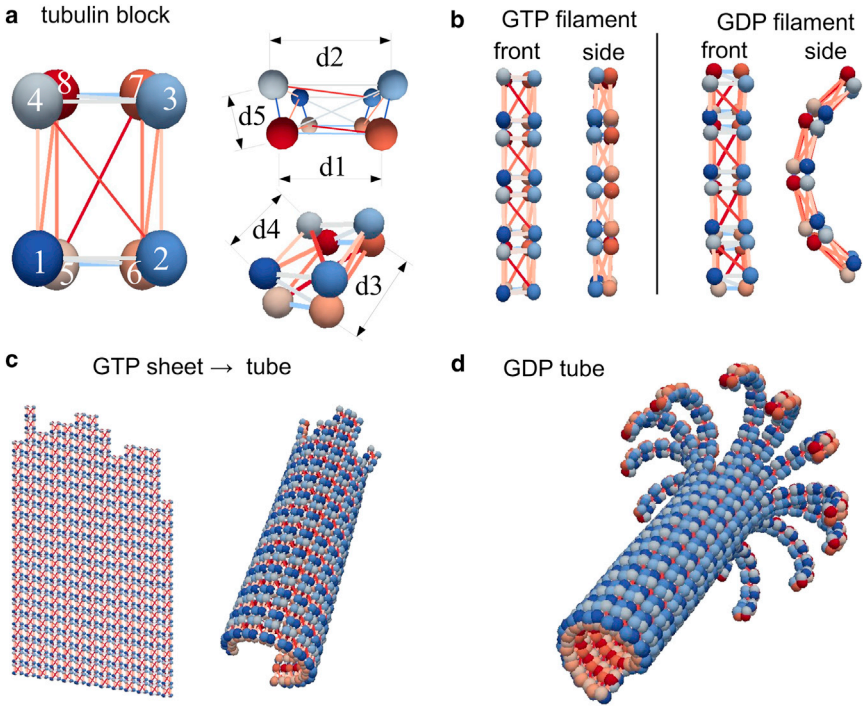

FIGURE 1 Three-dimensional tubulin block model of the MT. (*a*) A tubulin block consists of eight nodes connected to neighboring nodes via stiff linear springs. Diagonal struts are added to avoid shearing and twisting. Each node is also endowed with a hard-core repelling potential. The top and bottom faces of the blocks are of trapezoidal shape to induce lateral curvature in the MT. (*b*) A PF is obtained by arranging tubulin blocks along a line and connecting them with springs. PFs can be straight or bent, depending on the ratio of top/bottom lengths of the block. (*c*) A sheet of tubulin blocks will form a tubular structure when the opposing sides of the block are trapezoidal. In this case we have $d_2 > d_1$ and $d_3 = d_4$, corresponding to a GTP-bound MT. The sheet will fold with a helicity depending on the number of transversal units and the ratio d_2/d_1. (*d*) Clamping one end of the MT while hydrolyzing the blocks by letting $d_3 > d_4$ and allowing transversal bonds to break leads to the ram's-horn shape typical of depolymerizing MTs. To see this figure in color, go online.

MTs (14). Other estimates of the linear angular-spring stiffness of PFs yield slightly different values (48).

Finally, the particles composing the block are endowed with a hard-core repulsion potential (for numerical purposes, the repulsive part of a Lennard-Jones potential) with cutoff $r_{hc} = 5$ nm to avoid interpenetration of blocks. Longitudinal and transversal bond-lengths (d_{10} and d_{11}, respectively) are chosen smaller than the hard-core cutoff to avoid bond-deformation other than stretching. By allowing for bonds breaking and attachment, we can simulate polymerization and depolymerization processes. The model is implemented and simulated using the LAMMPS software package (LAMMPS Molecular Dynamics Simulator, http://lammps.sandia.gov/) (49).

Kinetochore-MT interface

We model the kinetochore-MT interface as an assembly of fibrils (16,17), which represent various candidate proteins and complexes (e.g., Ndc80, CENP-E, CENP-T, CENP-F) linked, e.g., by the Mis12 complex (18), the

TABLE 1 Parameters employed in three-dimensional simulations

Rest-length and stiffness of intra/intertubulin block springs

Edge	Symbol	Rest-length [nm]	Stiffness [pN/nm]	Notes
Intrablock	d_1	3.5	$k = 5 \times 10^6$	Incompressible blocks
	d_2	3.5–4.5	k	
	d_3	5.25–6.3	k	
	d_4	5.25	k	
	d_5	2.5	k	
Interblock	d_{10}	1.75	$k_{10} = (1.5–50) \times 10^5$	Calculation based on VanBuren et al. (14)
	d_{11}	1.75	$k_{11} = 50–1000$	and Mickey and Howard (47)

Constants used to describe kinetochore fibrils as bead-spring polymers

Constant	Symbol	Value	Notes
Stiffness	k_f	10^6 pN/nm	Taken to be inextensible
Bead size	r_b	2 nm	Thin compared to PFs
Maximal fibril length	l_0	20–50 nm	Estimated from McIntosh et al. (16,36)
Density	ρ_f	$0.77–3.8 \times 10^{-3}$ fibrils/nm^2	Estimate, Lawrimore et al. (50)

Lennard-Jones parameters for interactions of fibril tips

Interaction	E [pN/nm]	σ [nm]	r^* [nm]	Notes
Fibril-tip → fibril-tip	100–2000	2.5	3.75	Assumption: strong attraction
Fibril-tip → straight PF	1.5–5.00	7.5	30	Assumption: weak attraction
Fibril-tip → curved PF	500	7.5	7.5	Assumption: repulsion

Ska complex (43) or the Dam1 complex (20,21). Here the different proteins at the kinetochore-microtubule interface are treated on equal footing—coarse-grained into fibrils—and are modeled as bead-spring polymers of length $l_0 = 20$–50 nm (16,36). We consider hard-core repelling beads of radius $r_b = 2$ nm connected by linear springs of rest-length $2r_b$ and stiffness $k_f = 10^6$ pN/nm, which makes them practically inextensible. We also assume that fibrils have vanishing bending stiffness compared to the MTs. Kinetochore fibril bases are arranged randomly on a wide area with a density of $\rho_f = 0.77$–3.8×10^{-3} fibrils/nm^2 and then extended toward the incident MT-tip. In practice, these densities correspond to 10–50 fibrils per MT. The density was chosen based on the estimate of twenty Ndc80 complexes per captured MT (50). A summary of fibril parameters is reported in Table 1.

Fibril tips can bind either to tubulin blocks in a straight conformation or to other fibril tips. In our model, curling tubulin blocks cannot directly bind to fibrils, in agreement with experiments showing that the Ndc80 tip binds preferentially with straight tubulin conformations (28). This choice is made to illustrate the worst-case scenario, but it is expected that a weak attraction with curved tubulin filaments, possibly relevant for other protein complexes (e.g., CENP-E, CENP-T, Ska, CENP-F), would not change the results. Hence, an incident MT can attach to kinetochore fibrils either directly by binding to straight tubulin units or by locking curling PFs into fibril loops as shown in Fig. 2 *b*). In all cases, binding is implemented by a Lennard-Jones potential

$$V_{\mathrm{LJ}}(r) = 4\epsilon\left[\left(\frac{\sigma}{r}\right)^{12} - \left(\frac{\sigma}{r}\right)^{6}\right] r<r^*, \qquad (1)$$

where r^* is a cutoff, ϵ is the binding strength, and σ controls the width of the potential well. Note that fibrils in our model represent coarse-grained protein complexes so that their mutual interactions may reflect collective properties. Interaction with GDP-bound tubulin is modeled as a repulsive potential by setting $r^* = \sigma$. The parameters chosen for σ and r^* are chosen so that interpenetration between fibrils and blocks can be avoided (these parameters are reported in Table 1). Movie S1 in the Supporting Material illustrates the mechanism described here. It shows the result of a simulation where a straight MT enters a bundle of kinetochore filaments and binds some of them on its outer surface. When the MT protofilaments begin to curl and peel off the MT, some become entangled in loops formed by the kinetochore fibrils.

Simplified two-dimensional model of MT-protofilament elasticity

The three-dimensional model of the MT and the MT-kinetochore interface is highly complex and difficult to simulate for long times due to the stiffness of the bonds. Therefore, only limited results can be obtained by the full three-dimensional model. To obtain relevant statistics for the detachment kinetics, we need to perform some important approximation reducing the problem to two dimensions. Fig. 2 *d* suggests a way in which such a dimensional reduction might take place. The protofilament is modeled as a flexible chain of nodes connected via springs (15) with longitudinal stiffness $k = 15{,}000$ pN/nm and rest-length $a = 10$ nm (approximately one tubulin dimer). Because the fibrils form loops around the PF tip, the only way to detach, except for the dissociation of the fibril loop, is by sliding the loop off the PF ram's horn. In two dimensions, this process is illustrated in Fig. 2 *d*, where the cross-section of the fibrils is modeled as an elastic ball.

Here, we model the kinetics of a single protofilament attached to a substrate representing the interaction with neighboring protofilaments (13,15). The chain furthermore has an intrinsic bending angle of φ (17) and bending stiffness B. Hence, the elastic energy of a protofilament with node coordinates $\mathbf{r}_i$ is given by (15)

$$\mathcal{E}_{el,\mathrm{PF}} = \sum_i 1/2k(|\mathbf{r}_{i+1} - \mathbf{r}_i| - a)^2 - B/a\cos(\theta_i - \varphi) + H(r_c - y_i)1/2Sy_i, \qquad (2)$$

where $H(x)$ is the Heaviside step-function and the θ_i values are the angles between neighboring subunits. Hence, the elastic force on each node i is simply

$$\mathbf{f}^i_{el,\mathrm{PF}} = -\partial\mathcal{E}_{el,\mathrm{PF}}\Big/\partial\mathbf{r}_i.$$

As in the three-dimensional model, we estimate the bending stiffness of the PF from the flexural rigidity of a microtubule $EI_{\mathrm{MT}} \approx 10 \times 10^{-24}$ Nm^2 (see VanBuren et al. (14) and references therein) and its second moment of inertia $I_{\mathrm{MT}} \approx 2 \times 10^{-32}$ m^4 (47). Although the protofilament is modeled as a one-dimensional object, we estimate its model of inertia treating it as a cylinder of radius $b = 5$ nm, which yields $I_{\mathrm{PF}} \approx 10^{-34}$ m^4. By simple

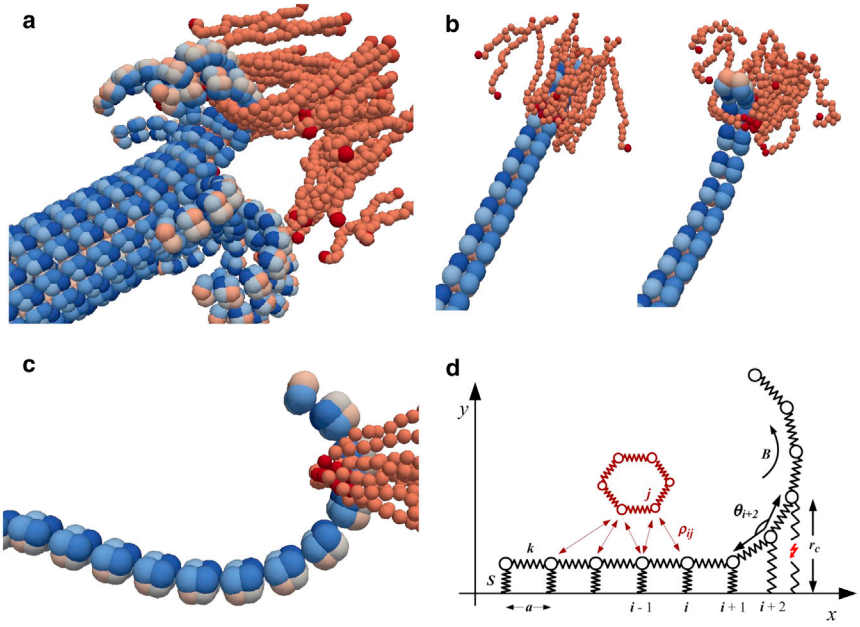

FIGURE 2 Summary of the model for the kinetochore-MT interface. (*a*) The fully hydrolyzed PFs of the MT curl, forming ram's horns, locking into loops formed by the kinetochore fibrils. (*b*) Genesis of a loop by fibrils attaching to the not-yet-hydrolyzed tubulin block, and locking into each other. When the tubulin blocks are hydrolyzed, the curling links the PF tip into the fibrils loop. (*c* and *d*) Side-view of a PF tip with kinetochore-fibril loops around it and its two-dimensional reduction. To see this figure in color, go online.

calculation we can then estimate $B = (EI_{MT}/I_{MT})I_{PF} \approx 5 \times 10^{-26}$ Nm^2. The interaction between the filament and the substrate is modeled by a spring with stiffness $S = 1000$ pN/nm, which breaks when it is extended beyond $r_c = 1$ nm. These parameters (S and r_c) were fitted to the requirement that depolymerizing MTs shrink at the experimentally observed speed, keeping a finite curvature at the tip to capture the fibrils. In fact, as shown in Zapperi and Mahadevan (15), only the combination $Sr^2{}_c$ rules the PF dynamics.

Two-dimensional simulations of fibril-MT interactions

As shown in Fig. 2 *d* we consider only the cross section of the fibril bundle (Fig. 2 *c*) and model it as a closed chain of six nodes connected by linear and angular springs with extension b, stretching stiffness k_f, and bending stiffness B_f. The elastic energy of the chain can then be written in a form equivalent to Eq. 2.

The interaction between the PF and the fibril is modeled by a repulsive potential in case of a depolymerizing MT and by an attractive force for a polymerizing MT: The repulsive force between each node of the depolymerizing PF $\mathbf{r}_i$ and the fibril $\mathbf{R}_j$ according to

$$\mathbf{f}^{ij}_{\text{int}} = -A\frac{\exp(-0.1\rho_{ij})}{\rho^3_{ij}}\mathbf{r}_{ij},$$

where $\mathbf{r}_{ij} = \mathbf{r}_i - \mathbf{R}_j$ and $\rho_{ij} = |\mathbf{r}_{ij}|$. The attractive interaction with polymerizing PF is modeled according to Eq. 1.

Numerical simulations of fibril-protofilament dynamics

The dynamics of the PF-fibril system is governed by the following coupled Langevin equations:

$$\gamma_{\text{PF}}\frac{d\mathbf{r}_i}{dt} = \mathbf{f}^i_{el,\text{PF}} + \mathbf{f}^{ij}_{\text{int}}, \tag{3a}$$

$$\gamma_f\frac{d\mathbf{R}_j}{dt} = \mathbf{f}^j_{el,f} - \mathbf{f}^{ij}_{\text{int}} + \mathbf{F} + \mathbf{G}_j. \tag{3b}$$

Here, γ_{PF} and γ_f are the damping coefficients of the nodes of the PF and the fibril, respectively, and $\mathbf{F} = F\hat{x}$ is an externally applied pulling force, acting along the horizontal direction. The thermal noise $\mathbf{G}_j$ acting on the fibril is a Gaussian random force with average $\langle \mathbf{G}_j(t)\rangle = 0$ and correlations

$$\left\langle \mathbf{G}_j(t)\mathbf{G}_k(t')\right\rangle = 2\gamma_f k_{\text{B}}T\delta_{ij}\delta(t-t'),$$

where T is the temperature and k_{B} is Boltzmann constant. In the following, we quantify the amplitude of thermal fluctuations by the parameter $\omega \equiv \sqrt{2k_{\text{B}}T/\gamma_f}$.

The damping coefficient can be evaluated considering that the drag coefficient of a sphere of radius r immersed in a fluid with dynamical viscosity η is given by the Stokes formula $\gamma = 6\pi\eta r$. The dynamical viscosity of water at $T \approx 300$ K is $\eta \approx 10^{-3}$ Pa s. Assuming that the radii of the fibril and PF are $r_f = 1$ nm and $r_{\text{PF}} = 10$ nm, we get $\gamma_f \approx 10^{-10}$ kg/s and $\gamma_{\text{PF}} \approx 10^{-9}$ kg/s. In these conditions, the thermal fluctuations of the PF are overshadowed by the interactions with the strongly fluctuating fibrils and can be safely dropped. This is particularly convenient because it further speeds up the simulations.

The MT shrinks or grows by adding or removing tubulin subunits from the tip, but in mammalian cells, MTs also depolymerize at the spindle poles that are associated with poleward flux of tubulin (51). Here, we consider that the PF is able to polymerize (attach subunits at the tip) or depolymerize (lose subunits from the tip) and switch between these states. The growing/shrinking velocities and switching rates we use are taken from experiments in the literature (29,52,53). We assume that the velocities are dependent on the force on the tip of the protofilament (29) according to

$$v_{g/s}(F) = v^0_{g/s} \times 10^{\pm F/F_{g/s}}. \tag{4}$$

Equations 3a and 3b are solved by a fourth-order Runge-Kutta algorithm for the PF and an Euler-Maruyama algorithm for the fibril. Due to numerical constraints, it is not possible to simulate the model over a timescale that is comparable to the experimental one. We thus artificially increase the noise fluctuations and then analyze how the results depend on ω. In this way, we are able to show that the numerical results approach the experimental ones because ω tends toward realistic values. The numerical values of the constants used in the simulations are summarized in Table 2.

RESULTS

Microtubule protofilaments entangle with kinetochore fibrils

We simulate the three-dimensional kinetochore-MT interface model presented and discussed in Materials and Methods. In Fig. 2 *a*, we show an MT whose curling PFs are partly linked into loops formed by kinetochore fibrils. In Fig. 2 *b* and Movie S2 we illustrate the process by which a curved PF locks into a loop formed by kinetochore fibrils.

TABLE 2 List of constants used in two-dimensional simulations

Name	Symbol	Values used	Comment
MT-protofilament			
Subunit length	a	10^{-8} m	Length scale
Drag coefficient	γ_{PF}	10^{-9} kg/s	Estimate
Bending stiffness	B	5×10^{-26} Nm^2	Calculation
Stretching stiffness	k	1.5×10^{-24} N/m	Assumption
Substrate stiffness	S	1.0×10^{-26} N/m	Fit
Breaking length	r_c	1 nm	Fit
Bending angle	φ	0.18–0.42	McIntosh et al. (17)
Growth velocity	v^0_{g}	0.008–0.21 μm/s	Akiyoshi et al. (29), Rusan et al. (52), and Tirnauer et al. (53)
Shrinking velocity	v^0_{s}	0.2–0.3 μm/s	Akiyoshi et al. (29) and Rusan et al. (52)
Growth acceleration	F_g	20 pN	Akiyoshi et al. (29)
Shrinking stall	F_s	7 pN	Akiyoshi et al. (29)
Rescue rate	$1/p_{\text{res}}$	0.045/s	Rusan et al. (52)
Catastrophe rate	$1/p_{\text{cat}}$	0.058/s	Rusan et al. (52)
Kinetochore fibril			
Segment length	b	10^{-9} m	Assumption
Drag coefficient	γ_f	10^{-10} kg/s	Estimate
Bending stiffness	B_f	5×10^{-27} Nm^2	Assumption
Stretching stiffness	k_f	10^{-25} N/m	Assumption
Fluctuation amplitude	ω	15–35 nm μs$^{-1/2}$	Tried values

A polymerizing PF, composed by straight tubulin blocks, reaches into the entangled kinetochore outer plate and fibrils attach to the tubulin blocks (see Fig. 2 *b*, *left*). Because fibril tips are now close together, they can easily bind with each other (as suggested in Ciferri et al. (27) and Zaytsev et al. (32)). When the PF depolymerizes and starts to curl, fibrils detach from the tubulin due to the reduced affinity, but the ram's horn of the PF can lock mechanically into the loop formed by the connected fibrils (see Fig. 2 *b*, *right*).

To test the fidelity of our kinetochore-microtubule interface model, we perform a series of simulations to see how many PFs are entangled in the fibril loops. The MT-tip was kept straight and moved into the mass of kinetochore fibrils with a velocity of 1 μm/min (53). Fibrils attach to the MT surface and bind to each other, especially when they are in proximity of the MT, thus forming loops. As soon as the tip of the longest PF reaches the area of the fibril bases, the incident velocity is set to zero, and the MT is set to depolymerize immediately. In this process, curling PFs can hook into the fibril loops. We perform this simulation for various fibril densities and average >30 realizations in each case. We report the number of entangled PFs as a histogram in Fig. 3 for 10, 20, and 50 fibrils per MT, or 0.77, 1.5, and 3.8 fibrils per PF. The average number of entangled PFs is 1.1, 4.5, and 5.2 for 10, 20, and 50 fibrils, respectively. Hence, even for a relatively small number of fibrils, there is significant and robust entanglement.

The geometrical conformations of the PF tips broadly correspond to the two distinct states of the dynamic MT—a growing/polymerizing (straight) and a shrinking/depolymerizing (curved) state, with differing chemistry and physics of the molecules at the tip. In the growing state, the tip of the MT recruits phosphorylyzed GTP-tubulin subunits, while the tubulin subunits in the rest of the MT body are progressively hydrolyzed. The main difference (for our purposes) between GTP and GDP-tubulin is the equilibrium angle between two connected subunits. Although a filament made out of GTP units tends to remain straight, a GDP-tubulin filament has a curved equilibrium configuration (see Fig. 1 *b*). As a consequence, the tips of PFs in a growing MT will tend to have rather straight configurations whereas in the depolymerizing phase, the PFs of the MT form hooks (ram's horns) while losing tubulin subunits.

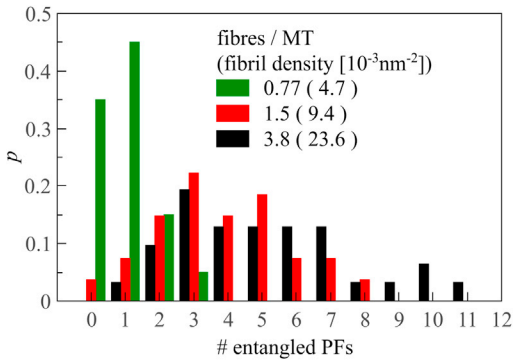

FIGURE 3 Histogram of the number of entangled PFs interacting with a set of kinetochore fibrils for three different densities. The total number of simulations is 30 in all cases. For details, see text. To see this figure in color, go online.

To estimate the load-carrying capacity of the MT-kinetochore interface, we consider only the tip of the PFs and assume that the constituting tubulin blocks are uniformly either hydrolyzed (GDP-bound) or phosphorylated (GTP-bound). In this way, we can discuss detachment from depolymerizing or polymerizing PFs separately and distinguish the underlying detachment mechanisms. In particular, a single PF is first inserted up to a few blocks, typically ranging from one to three, into a network of kinetochore fibrils and the system is then relaxed for 10 s. Because we always start from a GTP-tubulin PF, the tips of some fibrils bind to the outer side of the tubulin blocks (particles with 1–4; see Fig. 1 *a*). When the system is equilibrated, the distal end of the PF is held fixed, while the kinetochore plate, to which fibrils are attached, is moved with constant velocity $v = 10$ nm/s. In these conditions, we measure the longitudinal component (parallel to the pulling direction) of the interaction force between kinetochore and the PF.

For GTP-tubulin PFs, we plot the force-displacement curves in Fig. 4 *a* for three values of the binding strength ϵ(P-F) between fibrils and PFs. The fibril tips are, in this case, attached only to the first tubulin block of the PF (shown in the *inset*). The curves show the displacement *dy*, the difference between the starting and end positions of the kinetochore plate as a function of the in-line component of the interaction force, normalized to the number of attached fibrils. Simulations are repeated 30 times to average out the effect of thermal noise. The results show that at short displacements, the kinetochore plate feels no restoring force because the fibrils are unwrapped, i.e., straightened. At this point, attached fibrils finally exert a force on the plate due to the binding with the tubulin dimer, until the bond breaks. The detachment from a GTP-tubulin PF, therefore, relies solely on the attractive interaction between kinetochore fibrils and tubulin blocks. The process is illustrated in Movie S3.

When the PF is formed of GDP-tubulin, its end is curved and the fibril-tubulin interaction is turned into a purely repulsive potential. We perform the same simulation as detailed for the GTP-tubulin PF above. The difference is that the PF is inserted more than one tubulin block into the fibril network, typically two-to-four blocks, and the relaxation also entails the curling of the PF. We performed simulations for two values of the flexural rigidity and plot the results in Fig. 4 *b* (see also Movie S4). For the larger value of the stiffness, we observe pronounced oscillations of the force-displacement curve due to the sliding of the kinetochore fibrils on the tubulin blocks while uncurling. For the less stiff case, the oscillations are not clearly discernible and the detachment of the kinetochore-MT

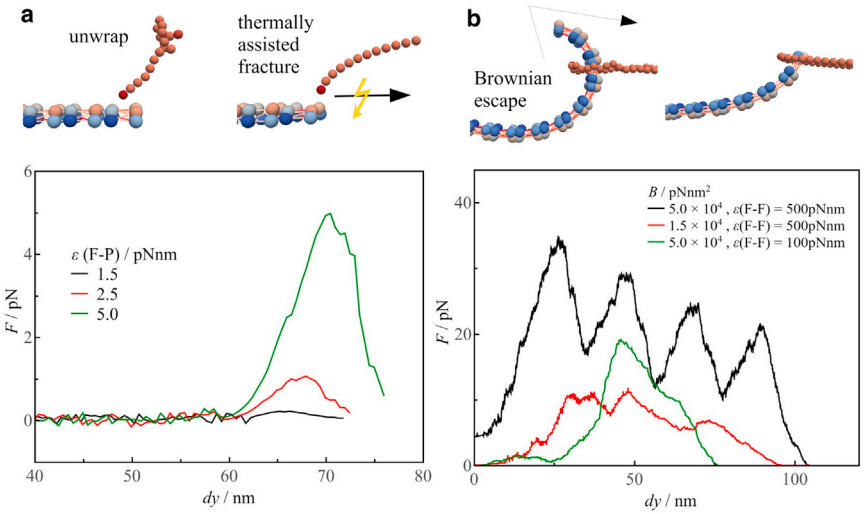

FIGURE 4 Detachment mechanisms of the kinetochore-PF interface. (*a*) Force-displacement curve of a straight PF-kinetochore fibrils interface. The fibrils are attached to the first tubulin block of the PF because the fibril tips interact with the PF via a Lennard-Jones potential with strength ϵ(F-P). Displacing the fibril ends leads at first to no increase of the force as long as the fibril unwraps. Upon completion of this straightening process, the force increases rapidly as the fibrils and the PF stretch while overcoming Lennard-Jones attraction. (*b*) Force-displacement curve of a GDP-tubulin PF in the curved conformation. Again, the kinetochore fibrils are pulled with constant velocity and the in-line component of the interaction force is plotted for flexural rigidity $B = 5 \times 10^4$ pN nm^2 and $B = 1.5 \times 10^4$ pN nm^2. The interaction energy between the fibrils is modeled by a Lennard-Jones potential with ϵ(F-F) = 500 pN nm or ϵ(F-F) = 100 pN nm. In the first case, the peak corresponds to the bending of the PF and in the second case, to the breakdown of the fibril loop. The oscillation (*black curve*) is due to the discrete nature of the PF and arises from the sliding of the kinetochore fibrils from one block to the next. This oscillation is drowned out by noise when the flexural rigidity is reduced (as shown in the *red curve*). To see this figure in color, go online.

interface is much smoother. As shown in Fig. 4 *b*, the peak load of a single depolymerizing PF is >10 pN, suggesting that a MT can, on average, carry a peak load of up to 50 pN, which compares nicely with experimental results (26). We also test the effect of the binding interactions between fibrils ϵ(F-F). For ϵ(F-F) = 100 pN nm and $B = 1.5 \times 10^4$ pN nm^2, the fibril loop eventually breaks (see Movie S5) but it is still able to carry a load of 20 pN. Hence for ϵ(F-F) = 100 pN nm and $B = 1.5 \times 10^4$ pN nm^2, the fibril loop should be strong enough to sustain a load of 20 pN, as we verified numerically.

A feature of the detachment not captured in the MD simulations is the thermally induced/assisted detachment that is prevalent at low forces. The reason is that thermal phenomena in a system such as ours appears on timescales much larger than we are able to simulate in three dimensions. To be able to simulate on statistically relevant timescales, we developed and implemented a two-dimensional equivalent of the kinetochore-MT interface, as already discussed in a previous section.

Shrinking microtubules form catch-bonds with kinetochore fibrils due to their conformation

For a shrinking PF, we assume that the fibrils do not attract to the tubulin molecules that are in curved conformation (28) but interact via a solely repulsive potential, as discussed in the Materials and Methods. To relate the experiments of Akiyoshi et al. (29) with the two-dimensional model, we chose an intrinsic bending angle of $\varphi = 0.36$, corresponding approximately to the peak of the curvature distribution measured experimentally in McIntosh et al. (17) and Alushin et al. (28). All the model parameters are reported in Table 2.

As described in the previous section, detachments can occur either because of thermal and other nonequilibrium fluctuations that lead the fibril to jump off the PF tip, or because a sufficiently strong pulling force mechanically bends the PF. In agreement with Akiyoshi et al. (29), low pulling forces increasingly stabilize the PF-fibril attachment. Furthermore, our model predicts that for larger forces, the attachment should again be destabilized. To compare the model with experiments, we plot in Fig. 5 *a* the numerical and experimental data for the detachment rate, denoted k_4 as in Akiyoshi et al. (29). The numerical data is plotted for various values of the fluctuation parameter ω. At small forces, the detachment rates is well fitted by exponential decay, $k_4 = k_4{}^0\exp(-F/F_4)$. The parameter F_4 follows an exponential curve as a function of ω, as shown in Fig. 5 *b*. From this plot we can extrapolate the value of ω in the experiment for our model and arrive at $\omega \approx 1$ nm μs$^{-1/2}$, which is a realistic and physical fluctuation parameter for this system. Hence, at low forces, simulations and experiments fit neatly together.

It is, however, unlikely that bond strengthening persists up to larger forces, where elastic deformation of the PF should take place. Indeed, simulations for large forces show that the lifetime of the kinetochore-microtubule attachment—the inverse of k_4—displays a peak at ~10 pN, and decreases very quickly after that, as shown in Fig. 5 *c*. The detachment times can be very well fitted at low forces and around the peak with a Weibull function

$$1/k_4(F) = \tau^0 + A_0\frac{k}{\lambda}\left(\frac{F}{\lambda}\right)^{k-1} e^{-(F/\lambda)^k}, \qquad (5)$$

where τ^0 is the lifetime at zero force, A_0 is the amplitude, and the Weibull parameters, λ and k, both depend on a

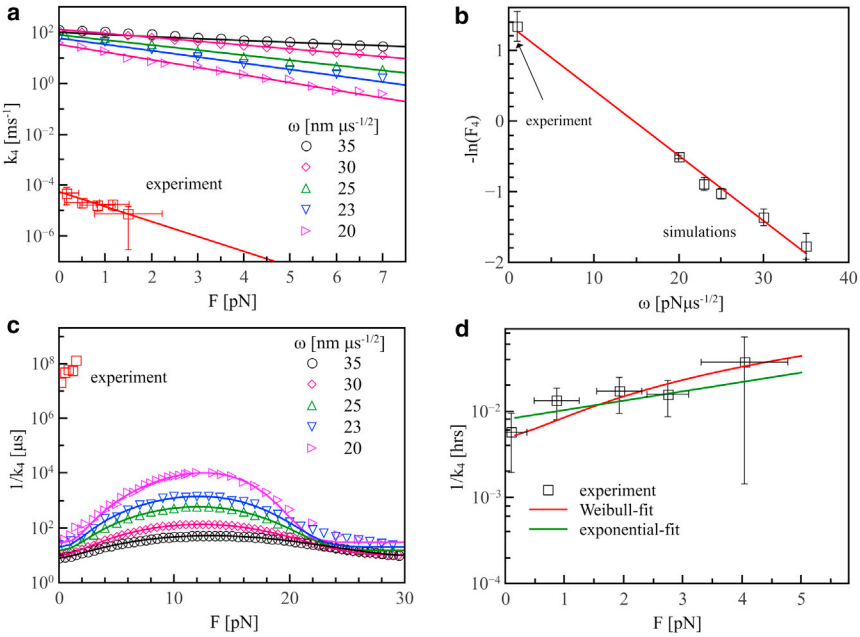

FIGURE 5 Simulation of the catch-bond behavior for depolymerizing PFs. (*a*) The detachment rate as a function of the pulling force for different values of the diffusion parameter ω for the two-dimensional model of a depolymerizing PF together with the experimental data from Akiyoshi et al. (29). (*b*) Extrapolation of the diffusion parameter ω in the experiments from the numerical data. (*c*) Attachment lifetimes (inverse detachment rates) of depolymerizing PFs to kinetochores at high forces. The numerical data suggests that the lifetime peaks due to deformations and then decreases sharply with applied load. The low-force parts and the peaks can be fitted well with the Weibull distribution, which yields also a reasonable fit for the experimental data, as shown in panel *d*. To see this figure in color, go online.

diffusion parameter ω. The Weibull function also provides an alternate fit for the lifetime of attachments with depolymerizing PFs in the experimental data, as shown in Fig. 5 *d*, together with the original exponential fit. Both fits yield consistent results, but it is difficult to decide which one is better. In both cases, the reduced χ^2 resulting from least-square minimization is $\sim 10^{-5}$, which is a clear indication of overfitting.

Our model suggests that measuring the lifetime of depolymerizing MT attachments to kinetochores should result in a peak at larger forces. As mentioned before, detachments at large force are due to a different physical process than the detachments at low forces. In Akiyoshi et al. (29), the destabilization of the kinetochore-MT attachment was attributed to a switch of the MT from the shrinking to the growing state. Although we do not discount that possibility, we suggest the existence of an alternate pathway that could be dominant at short timescales: When the pulling force is large enough, the depolymerizing PF is uncurled (see Movie S2).

Growing microtubules display force-weakening bonds ruled by the binding affinity with kinetochore fibrils

In the two-dimensional model, kinetochore fibrils are pulled with a constant force, while the PF is growing or shrinking. The time-frame for switching between the two states is much larger than the detachment times we are able to simulate, and therefore the effects of rescue and catastrophe do not affect our numerical results. To further simplify the numerical simulation and thus the results for longer times, we model the detachment from polymerizing PFs as a simple escape from a Lennard-Jones potential with a cutoff and simulate Eq. 3b. We have tested in some specific cases that the results are indistinguishable from those obtained with the complete model.

The result for various values, as plotted in Fig. 6 *a*, reports the value of the attachment lifetime (denoted by k_3 as in Akiyoshi et al. (29)) obtained in simulations as a function

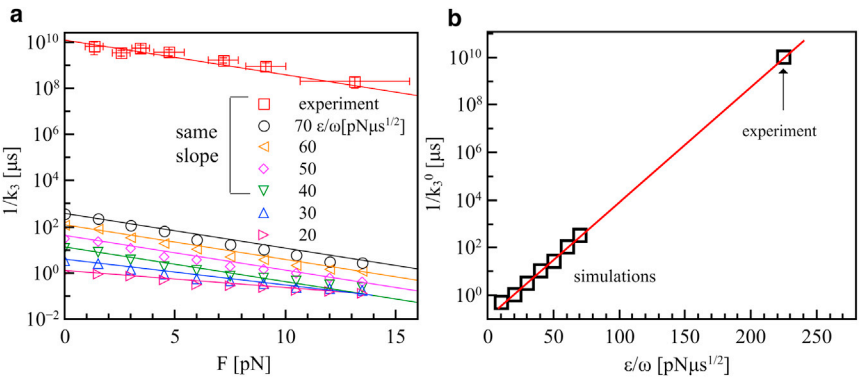

FIGURE 6 Detachment from a growing PF. (*a*) Attachment lifetimes obtained for the two-dimensional model for polymerizing PFs as a function of the binding strength-fluctuation ratio ϵ/ω together with the experimental data from Akiyoshi et al. (29). For a sufficiently high binding strength/fluctuation ratio, the parameter F_3, appearing as the slope here, stays constant and is the same for the numerical and experimental data. (*b*) Extrapolation of the experimentally observed binding strength. To see this figure in color, go online.

of the binding energy-fluctuation ratio ϵ/ω together with the experimental data. Numerical simulations and experimental data are well fitted with exponential curves, and have the same slope on a logarithmic scale. In particular, we fit the rate as

$$k_3(F) = k_3^0(\epsilon/\omega)\exp(F/F_3), \quad (6)$$

where only the detachment rate at zero force $k^0{}_3$ depends on the ratio ϵ/ω, while $F_3 \approx 3.8$ pN is the same for experimental and numerical data. Plotting $1/k^0{}_3$ vs. ϵ/ω for the numerical result allows us to extrapolate the ϵ/ω value for the experiment, $\epsilon/\omega \approx 225$ pN $\mu s^{1/2}$, as shown in Fig. 6 *b*. Because we previously estimated $\omega \approx 1$ nm $\mu s^{-1/2}$ for the experiment, we predict the attachment strength of the fibrils to the kinetochore to be $\epsilon \approx 225$ pN nm $\approx 50\, k_B T$. This is of the order of magnitude for usual protein-protein interactions, providing an additional confirmation of the validity of our approach.

Protofilament intrinsic curvature can determine the stability of MT-kinetochore attachments

The main point of cell division is the segregation of replicated chromosomes into two daughter cells. This is chiefly executed by the mitotic spindle, consisting of MTs, organized into two astral structures whose centers derive from centrosomes and associated proteins. Faithful segregation of the chromosomes requires proper biorientation, and thus dynamic kinetochore-MT attachments (i.e., erroneous attachments such as kinetochores attached to an MT emanating from the wrong pole) must be allowed for, and then corrected. In other words, kinetochore-MT attachments can be unstable or stable, short-lived or long-lived.

For a given value of the diffusion amplitude ω, we can vary φ and plot the detachment times with respect to constant pulling force. We see that the peak height as well as the offset τ_0 decrease with φ, and at a critical value the detachment time at zero force $\tau_0 = t(F = 0)$ is higher than the peak. Decreasing φ further makes the peak disappear completely and we end up with a detachment curve that is purely exponentially decreasing with applied force. As an example, we plot in Fig. S1 *a* in the Supporting Material the detachment times for $\omega = 20$ nm $\mu s^{-1/2}$ for a set of values of φ. As φ decreases, the catch-bond peak is reduced, and is shifted to smaller forces. At a critical value—for $\omega = 20$ nm $\mu s^{-1/2}$, it is $\varphi = 0.275$—the peak detachment time is at the same height as the zero-force detachment time $\tau_0 = t(F_{peak})$. Then, the peak completely disappears for $\varphi < 0.15$ and the detachment curve is a simple exponential decay. These observations allow us to construct a very simple phase diagram where the transition line corresponds to the condition for which the catch-bond disappears. In the stable region, the attachment time increases with small applied forces, while it decreases in the unstable region. An example for $B = 5 \times 10^4$ pN nm^2 and $\omega = 20$ is shown in Fig. S1 *b*. A stable region for $\varphi > 0.275$ (*right dash*) and an unstable region for $\varphi < 0.275$ splits into a weak part (*left dash*), where $\tau_{peak} < \tau_0$ and then a truly unstable part (*cross dash*) with no peak at all. The same procedure can be repeated for different values of ω, allowing us to construct a phase diagram for the stability of the attachment that we report in Fig. S2.

DISCUSSION

A conformational mechanism for the catch-bond

Our model for MT-kinetochore attachments captures and explains in easy-to-understand terms several key features of experimentally observed phenomena. Most prominently, we could reproduce the detachment times of MTs from kinetochores that are pulled with constant force (29). Using the model, we simulate the emergence of the catch-bond—the stabilization by tension—of the kinetochore interface with a depolymerizing protofilament, emphasizing the role of the geometrical conformation of the kinetochore-microtubule interface.

We identified different mechanisms of kinetochore-microtubule detachment for straight and curled protofilament tips, as follows.

1. Kinetochore fibrils are attached to straight protofilaments and detach due to thermal activation. This detachment is facilitated by an applied force, resulting in exponential weakening of the attachment.
2. Neighbor fibrils that have attached to each other form loops into which curling protofilaments hook. When no external force is applied, the loop can escape by thermal fluctuations, i.e., Brownian motion.
3. When the loop and PF-tip are pulled apart, the thermal fluctuations acquire a bias to move preferentially toward the tip of the PF, making an escape from a ram's-horn conformation more unlikely, thereby stabilizing the attachment. However, if the pulling force is too strong, then the ram's horn becomes uncurled or the loop breaks, so that the attachment is destabilized again.

The third point makes an experimental prediction—at higher forces, the detachment rate from depolymerizing PFs increases again—which could be easily be confirmed experimentally. Accordingly, one should extend the experiments plotted in Fig. 4c of Akiyoshi et al. (29) to measure the detachment rate from depolymerizing MTs at higher forces. The two-state model of Akiyoshi et. al. implicitly assumes that the detachment rate should continue to decrease with applied force, while our model predicts that it should eventually go up.

Geometrical aspects of MT-kinetochore attachment stability

Another prediction that follows from our results is the stabilization of kinetochore-MT attachments via the intrinsic

curvature of the MT protofilaments. The simulations show that the higher the PF curvature, the longer the lifetime of the attachment. If the intrinsic curvature is small enough, the stabilization, together with the catch-bond, then disappears and the attachment becomes weaker with applied force. In our model, the duration of kinetochore-MT attachments depends heavily on the flexural rigidity and intrinsic curvature of the PFs. In particular, our model suggests that a variation of the intrinsic curvature φ can cause a switch between stable/unstable attachments of depolymerizing PFs from kinetochores. This seems reasonable, because there is a broad distribution of bending angles found in experiments (17). Although the intrinsic curvature of a PF in isolation would be solely determined by the angle and stiffness between GTP/GDP-tubulin blocks, it is not unreasonable to assume that other factors influence the mechanical properties of protofilaments, and thereby regulate the stability of the kinetochore-MT interface.

Our model, therefore, naturally suggests an additional path to vary the type of the attachment from stable to unstable, and vice versa. This mechanical process can of course be seen as complementary to any other accompanying process, such as, for example, the stability regulation by Ndc80 (54) and Aurora B (55) or the switch of the MT state from growing to shrinking (29). In particular, the breakdown of the catch-bond could also occur according to two additional pathways: 1), the dissociation of fibril loops and 2), the fracture of MT-PFs. A possible hypothesis is that Aurora B is responsible for the dissociation of fibril loops because it phosphorylates the terminal ends of the Ndc80 complex (54). To the best of our knowledge, the influence of chemical or biological agents on the elastic properties of MTs and PFs and their tips has not been studied and it will be exciting to see whether future experiments prove our predictions.

Comparison with other models

Earlier models for the kinetochore-microtubule interface make use of the curling of PFs to show how force can be produced by the geometry of the protofilament (35,39,48). These studies focus mainly on the load-bearing capabilities of the PFs and do not go into detail on the mechanism of the coupling to the kinetochore. Our work builds on these insights, but we do include some very recent experimental results into our model, allowing us to explore the kinetochore interface in more detail, and make some specific predictions based on them.

In contrast to the biased-diffusion based Hill sleeve (33,34) or the motor-protein-based (40) models, our model does not investigate the biochemical aspects of the kinetochore-MT interface, but focus instead on its mechanics. The biochemical properties of the interface that are needed, i.e., the fibril-tip attachment strength to neighbor fibril tips and the MT surface, are not readily available and have to be fit. We furthermore investigate phenomena that are slightly different from the chromosome transport and breathing for which these models were designed. Our model sheds light instead on the genesis of the kinetochore-MT interface together with the role of the geometrical conformation of the PF tips.

An approach that is similar in spirit to ours was recently published in Zaytsev et al. (32). There the authors also model the collective action of kinetochore fibrils on the MTs, but the methodology employed is quite different. While in that article the authors explore the kinetochore-MT interface in a mean-field approximation using rate equations, we simulate directly the movement of each fibril and its interactions with the MT separately and then look at the emergent behavior. Tellingly, in both studies the cooperation of kinetochore fibrils is found to be essential to strengthen and stabilize the interface. Another difference, of course, is that we explicitly make use of the geometrical details of the protofilament curl and base predictions of the emergence of the kinetochore-microtubule interface upon it.

Our results fit neatly between different facets of the study of the kinetochore-microtubule interface and condense established experimental results into what we believe to be a new kind of model. Using molecular and stochastic dynamics simulations, we are able to elucidate and predict some very new aspects of the attachment of kinetochore fibrils to microtubule protofilaments.

CONCLUSIONS

In this article, we introduce a computational model of the kinetochore-microtubule interface that is based on the synthesis of different experimental observations. It showed that fibrils extend from the kinetochore and capture MT tips (16,36); kinetochore proteins form entangled networks (18); the essential kinetochore protein complex Ndc80 interacts in different ways with curved and straight protofilaments (28); and that Ndc80 complexes bind to each other (27). Hence, we assume that individual kinetochore fibrils are composed by different essential protein-complexes and can be treated as building blocks for the kinetochore-MT interface. We then employ a three-dimensional MT model treating the tubulin hetero-dimers as wedge-shaped blocks that can have configurations corresponding to either GTP- or GDP-bound tubulin. The tubulin blocks organize into protofilaments with intrinsic curvature (GDP-tubulin) or without (GTP-tubulin). The kinetochore fibrils are modeled as bead-spring polymers that can attach to the top-side of straight protofilaments. The fibril tips also attach to each other, forming effective loops into which curling protofilament-tips can hook.

The computational model provides a clear illustration of how the conformation of MT-PFs influences the stability of their attachments with the kinetochore in a manner that is quite general and robust. Besides its application to the experiments reported in Akiyoshi et al. (29), our model

represents a general computational tool that could be useful to guide future experimental investigations of MT-kinetochore interactions.

SUPPORTING MATERIAL

Two figures and five movies are available at http://www.biophysj.org/biophysj/supplemental/S0006-3495(14)00606-7.

We thank Zoe Budrikis and Alessandro Sellerio for useful discussions and comments.

Z.B. and S.Z. are supported by the European Research Council through Advanced Grant "SIZEFFECTS". Work in the laboratory of H.M. is funded by Le Fonds Européen de Développement Régional (FEDER) through the Operational Competitiveness Program "COMPETE" and by National Funds through the Fundacão para a Ciência e a Tecnologia under project No. FCOMP-01-0124-FEDER-015941 (grant No. PTDC/SAU-ONC/112917/2009), the Human Frontier Science Program, and the Seventh Framework Program grant "PRECISE" from the European Research Council.

REFERENCES

1. Cheeseman, I. M., and A. Desai. 2008. Molecular architecture of the kinetochore-microtubule interface. *Nat. Rev. Mol. Cell Biol.* 9:33–46.
2. Abbas, T., M. A. Keaton, and A. Dutta. 2013. Genomic instability in cancer. *Cold Spring Harb. Perspect. Biol.* 5:a012914.
3. Biggins, S., and A. W. Murray. 2001. The budding yeast protein kinase Ipl1/Aurora allows the absence of tension to activate the spindle checkpoint. *Genes Dev.* 15:3118–3129.
4. Lampson, M. A., and I. M. Cheeseman. 2011. Sensing centromere tension: Aurora B and the regulation of kinetochore function. *Trends Cell Biol.* 21:133–140.
5. Tanaka, T. U., N. Rachidi, …, K. Nasmyth. 2002. Evidence that the Ipl1-Sli15 (Aurora kinase-INCENP) complex promotes chromosome bi-orientation by altering kinetochore-spindle pole connections. *Cell.* 108:317–329.
6. Mitchison, T., and M. Kirschner. 1984. Dynamic instability of microtubule growth. *Nature.* 312:237–242.
7. Müller-Reichert, T., D. Chrétien, …, A. A. Hyman. 1998. Structural changes at microtubule ends accompanying GTP hydrolysis: information from a slowly hydrolyzable analogue of GTP, guanylyl (α,β)methylenediphosphonate. *Proc. Natl. Acad. Sci. USA.* 95:3661–3666.
8. Wang, H. W., and E. Nogales. 2005. Nucleotide-dependent bending flexibility of tubulin regulates microtubule assembly. *Nature.* 435: 911–915.
9. Chrétien, D., I. Jáinosi, …, H. Flyvbjerg. 1999. Microtubule's conformational cap. *Cell Struct. Funct.* 24:299–303.
10. Kis, A., S. Kasas, …, L. Forró. 2002. Nanomechanics of microtubules. *Phys. Rev. Lett.* 89:248101.
11. Hunyadi, V., and I. M. Jánosi. 2007. Metastability of microtubules induced by competing internal forces. *Biophys. J.* 92:3092–3097.
12. Jánosi, I. M., D. Chrétien, and H. Flyvbjerg. 1998. Modeling elastic properties of microtubule tips and walls. *Eur. Biophys. J.* 27:501–513.
13. Jánosi, I. M., D. Chrétien, and H. Flyvbjerg. 2002. Structural microtubule cap: stability, catastrophe, rescue, and third state. *Biophys. J.* 83:1317–1330.
14. VanBuren, V., L. Cassimeris, and D. J. Odde. 2005. Mechanochemical model of microtubule structure and self-assembly kinetics. *Biophys. J.* 89:2911–2926.
15. Zapperi, S., and L. Mahadevan. 2011. Dynamic instability of a growing adsorbed polymorphic filament. *Biophys. J.* 101:267–275.
16. McIntosh, J. R., E. L. Grishchuk, …, F. I. Ataullakhanov. 2008. Fibrils connect microtubule tips with kinetochores: a mechanism to couple tubulin dynamics to chromosome motion. *Cell.* 135:322–333.
17. McIntosh, J. R., E. O'Toole, …, E. L. Grishchuk. 2013. Conserved and divergent features of kinetochores and spindle microtubule ends from five species. *J. Cell Biol.* 200:459–474.
18. Dong, Y., K. J. Vanden Beldt, …, B. F. McEwen. 2007. The outer plate in vertebrate kinetochores is a flexible network with multiple microtubule interactions. *Nat. Cell Biol.* 9:516–522.
19. Schmidt, J. C., H. Arthanari, …, I. M. Cheeseman. 2012. The kinetochore-bound Ska1 complex tracks depolymerizing microtubules and binds to curved protofilaments. *Dev. Cell.* 23:968–980.
20. Tanaka, K., E. Kitamura, …, T. U. Tanaka. 2007. Molecular mechanisms of microtubule-dependent kinetochore transport toward spindle poles. *J. Cell Biol.* 178:269–281.
21. Volkov, V. A., A. V. Zaytsev, …, E. L. Grishchuk. 2013. Long tethers provide high-force coupling of the Dam1 ring to shortening microtubules. *Proc. Natl. Acad. Sci. USA.* 110:7708–7713.
22. Westermann, S., A. Avila-Sakar, …, G. Barnes. 2005. Formation of a dynamic kinetochore- microtubule interface through assembly of the Dam1 ring complex. *Mol. Cell.* 17:277–290.
23. Westermann, S., H. W. Wang, …, G. Barnes. 2006. The Dam1 kinetochore ring complex moves processively on depolymerizing microtubule ends. *Nature.* 440:565–569.
24. Koshland, D. E., T. J. Mitchison, and M. W. Kirschner. 1988. Polewards chromosome movement driven by microtubule depolymerization in vitro. *Nature.* 331:499–504.
25. Grishchuk, E. L., and J. R. McIntosh. 2006. Microtubule depolymerization can drive poleward chromosome motion in fission yeast. *EMBO J.* 25:4888–4896.
26. Grishchuk, E. L., M. I. Molodtsov, …, J. R. McIntosh. 2005. Force production by disassembling microtubules. *Nature.* 438:384–388.
27. Ciferri, C., S. Pasqualato, …, A. Musacchio. 2008. Implications for kinetochore-microtubule attachment from the structure of an engineered Ndc80 complex. *Cell.* 133:427–439.
28. Alushin, G. M., V. H. Ramey, …, E. Nogales. 2010. The Ndc80 kinetochore complex forms oligomeric arrays along microtubules. *Nature.* 467:805–810.
29. Akiyoshi, B., K. K. Sarangapani, …, S. Biggins. 2010. Tension directly stabilizes reconstituted kinetochore-microtubule attachments. *Nature.* 468:576–579.
30. Marshall, B. T., M. Long, …, C. Zhu. 2003. Direct observation of catch bonds involving cell-adhesion molecules. *Nature.* 423:190–193.
31. Thomas, W. E., V. Vogel, and E. Sokurenko. 2008. Biophysics of catch bonds. *Annu. Rev. Biophys.* 37:399–416.
32. Zaytsev, A. V., F. I. Ataullakhanov, and E. L. Grishchuk. 2013. Highly transient molecular interactions underlie the stability of kinetochore – microtubule attachment during cell division. *Cell Mol. Bioeng.* 6: 393–405.
33. Hill, T. L. 1985. Theoretical problems related to the attachment of microtubules to kinetochores. *Proc. Natl. Acad. Sci. USA.* 82:4404–4408.
34. Joglekar, A. P., and A. J. Hunt. 2002. A simple, mechanistic model for directional instability during mitotic chromosome movements. *Biophys. J.* 83:42–58.
35. Efremov, A., E. L. Grishchuk, …, F. I. Ataullakhanov. 2007. In search of an optimal ring to couple microtubule depolymerization to processive chromosome motions. *Proc. Natl. Acad. Sci. USA.* 104: 19017–19022.
36. McIntosh, J. R., V. Volkov, …, E. L. Grishchuk. 2010. Tubulin depolymerization may be an ancient biological motor. *J. Cell Sci.* 123: 3425–3434.
37. Molodtsov, M. I., E. L. Grishchuk, …, F. I. Ataullakhanov. 2005. Force production by depolymerizing microtubules: a theoretical study. *Proc. Natl. Acad. Sci. USA.* 102:4353–4358.

38. Shtylla, B., and D. Chowdhury. 2013. A theoretical model for attachment lifetimes of kinetochore-microtubules: mechano-kinetic catch-bond mechanism for error-correction. arXiv:1301.5692v2 [physics.bio-ph].

39. Shtylla, B., and J. P. Keener. 2011. A mathematical model for force generation at the kinetochore-microtubule interface. *SIAM J. Appl. Math.* 71:1821–1848.

40. Civelekoglu-Scholey, G., D. J. Sharp, …, J. M. Scholey. 2006. Model of chromosome motility in *Drosophila* embryos: adaptation of a general mechanism for rapid mitosis. *Biophys. J.* 90:3966–3982.

41. Gudimchuk, N., B. Vitre, …, E. L. Grishchuk. 2013. Kinetochore kinesin CENP-E is a processive bi-directional tracker of dynamic microtubule tips. *Nat. Cell Biol.* 15:1079–1088.

42. Suzuki, A., T. Hori, …, T. Fukagawa. 2011. Spindle microtubules generate tension-dependent changes in the distribution of inner kinetochore proteins. *J. Cell Biol.* 193:125–140.

43. Abad, M. A., B. Medina, …, A. A. Jeyaprakash. 2014. Structural basis for microtubule recognition by the human kinetochore Ska complex. *Nat. Commun.* 5:2964.

44. Hunyadi, V., D. Chrétien, …, I. M. Jánosi. 2007. Why is the microtubule lattice helical? *Biol. Cell.* 99:117–128.

45. Cheng, S., A. Aggarwal, and M. J. Stevens. 2012. Self-assembly of artificial microtubules. *Soft Matter.* 8:5666–5678.

46. Cheng, S., and M. J. Stevens. 2014. Self-assembly of chiral tubules. *Soft Matter.* 10:510–518.

47. Mickey, B., and J. Howard. 1995. Rigidity of microtubules is increased by stabilizing agents. *J. Cell Biol.* 130:909–917.

48. Molodtsov, M. I., E. A. Ermakova, …, F. I. Ataullakhanov. 2005. A molecular-mechanical model of the microtubule. *Biophys. J.* 88: 3167–3179.

49. Plimpton, S. 1995. Fast parallel algorithms for short-range molecular dynamics. *J. Comput. Phys.* 117:1–19.

50. Lawrimore, J., K. S. Bloom, and E. D. Salmon. 2011. Point centromeres contain more than a single centromere-specific Cse4 (CENP-A) nucleosome. *J. Cell Biol.* 195:573–582.

51. Mitchison, T. J. 1989. Polewards microtubule flux in the mitotic spindle: evidence from photoactivation of fluorescence. *J. Cell Biol.* 109: 637–652.

52. Rusan, N. M., C. J. Fagerstrom, …, P. Wadsworth. 2001. Cell cycle-dependent changes in microtubule dynamics in living cells expressing green fluorescent protein-α tubulin. *Mol. Biol. Cell.* 12:971–980.

53. Tirnauer, J. S., J. C. Canman, …, T. J. Mitchison. 2002. EB1 targets to kinetochores with attached, polymerizing microtubules. *Mol. Biol. Cell.* 13:4308–4316.

54. DeLuca, J. G., W. E. Gall, …, E. D. Salmon. 2006. Kinetochore microtubule dynamics and attachment stability are regulated by Hec1. *Cell.* 127:969–982.

55. Cimini, D., X. Wan, …, E. D. Salmon. 2006. Aurora kinase promotes turnover of kinetochore microtubules to reduce chromosome segregation errors. *Curr. Biol.* 16:1711–1718.